Journal of Materials Science & Technology 67 (2021) 11–22

Contents lists available at ScienceDirect

Journal of Materials Science & Technology

journal homepage: www.jmst.org

Research Article

Numerical investigation of a novel pattern for reducing residual stress in metal additive manufacturing

Li Sun [a], Xiaobo Ren [b], Jianying He [a], Zhiliang Zhang [a,*]

[a] Department of Structural Engineering, Norwegian University of Science and Technology (NTNU), Trondheim 7491, Norway
[b] SINTEF Industry, Trondheim 7456, Norway

ARTICLE INFO

Article history:
Received 29 March 2020
Received in revised form 19 May 2020
Accepted 25 May 2020
Available online 7 August 2020

Keywords:
Additive manufacturing (AM)
Deposition pattern
Temperature distribution
Residual stress
Warpage

ABSTRACT

Deposition patterns can significantly affect residual stress distribution in additive manufacturing processes. In this paper, a novel pattern, the S-pattern, is proposed for the metal additive manufacturing process. The finite element method is used to study the temperature field and the stress field of a cuboid structure under the S-pattern and five other representative patterns: zig-zag, raster, alternate-line, in-out spiral, and out-in spiral. The results show that the S-pattern achieves the lowest values of both equivalent residual stress and maximum principal residual stress, and the warpage of the S-pattern is close to that of counterparts. By analyzing the temperature and stress fields under all patterns, it is found that the residual stress distribution is determined by the uniformity of temperature distribution which is correlated with the peak temperatures of corners. The equivalent residual stress and the maximum principal residual stress are inversely correlated with the average peak temperature and the minimum peak temperature of corners, respectively. These correlations between temperature and residual stress provide an effective approach to evaluate the residual stress of different patterns and guide the deposition process in practice.

1. Introduction

Additive manufacturing (AM) can be used to print a product by successively adding the material layer by layer guided by a three-dimensional digital model [1,2]. According to the feedstock delivery system, AM can be divided into two categories: directed energy deposition and powder bed fusion [3]. For both processes, the powder or wire is melted by a focused energy source and consolidated rapidly [4]. Residual stress and residual deformation will inevitably be induced by temperature gradient, which will worsen fatigue and fracture resistance, and even lead to the failure of components [5]. As one of the key challenges in AM, residual stress is significantly influenced by the printing process [6]. Hence, the optimization of the printing processes for reducing residual stress and deformation is a critical issue.

Scanning or deposition pattern has a remarkable effect on residual stress since it influences the transient temperature distribution in the printing process greatly [7]. It is an essential and complex issue for AM because it affects many other aspects, such as deformation, part strength, fabrication quality, and deposition efficiency. In the present study, six representative basic patterns are used for AM, raster, zig-zag, alternate-line, in-out spiral, out-in spiral [8], and fractal, as shown in Fig. 1. The raster, zig-zag and alternate-line are direction-parallel patterns, while out-in spiral and in-out spiral are the contour-parallel patterns. The direction-parallel patterns are most commonly used due to good product quality, simple planning algorithms and wide applicability for various structures. Among them, the raster is the most popular pattern for the directed energy deposition process. The alternate line pattern is derived from the raster pattern, in which the passes are alternate and the accumulation of heat can be depressed, so that the temperature gradient and the residual stress are reduced. However, it is insufficient due to the need of the intervals between deposition passes. The zig-zag pattern is more efficient than the raster pattern because of fewer starts and stops of the energy source, which is the most common approach in commercial AM systems [9]. Due to the excessive accumulation at the turning points of the patterns, precise control of process parameters is required for the zig-zag pattern [7]. In contrast, the contour-parallel patterns are continuous but they are not suitable for filling patterns. They are not allowed to generate weave patterns which is helpful to reduce defects and improve the strength. In order to obtain both good geometric accuracy and

* Corresponding author.
E-mail address: zhiliang.zhang@ntnu.no (Z. Zhang).

https://doi.org/10.1016/j.jmst.2020.05.080

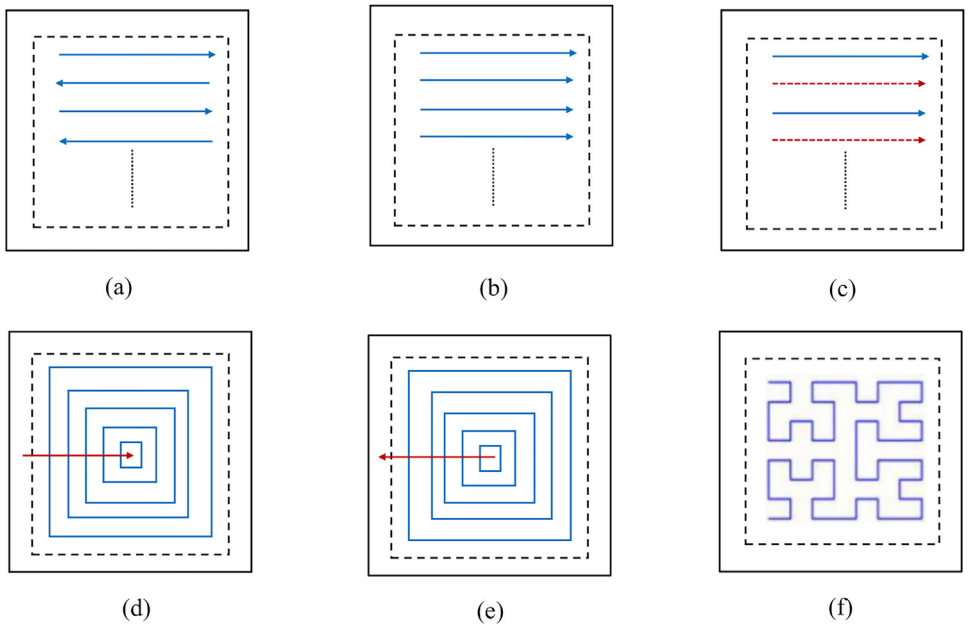

Fig. 1. Representative deposition patterns: (a) Zig-zag; (b) Raster; (c) Alternate-line; (d) Out-in spiral; (e) In-out spiral; (f) Hilbert.

high construction efficiency, the combination of contour-parallel patterns and zig-zag pattern is developed, and the contour and zig-zag patterns are applied to fill the internal area and the boundary area of the part, respectively [10,11]. The fractal pattern is still at the primary stage of the application as it is only used in the laser process due to many corners [7].

Many researchers have studied residual stresses and warpage under different patterns [7,[12–18,20],[12–18,20][49]]. The cuboid structures with rectangular or square section, thin-walled, enclosed, and cross structures were investigated, and the factors affecting residual stress and warpage were analyzed. Most studies focused on the width-wise zig-zag, length-wise zig-zag, out-in spiral, and in-out spiral patterns. Among direction-parallel patterns, the width-wise zig-zag pattern showed the maximum residual stress and distortion, while the length-wise zig-zag pattern resulted in lower distortion due to more homogeneous temperature distribution. For contour-parallel patterns, the out-in spiral resulted in higher residual stresses because the heat was accumulated inward and concentrated in the center part as the deposition process, while the heat dissipated outward and thus the temperature distribution was more homogeneous under in-out spiral pattern [21]. Many studies have investigated the effect of pattern element length on the residual stress and concluded that a shorter element could lower the residual stress and the island scanning could reduce the residual stress and part deformation [16,22–25]. Schröffer et al. [26] proposed the island planning strategy which achieved more homogeneous temperature and stress distributions. Zaeh et al. [27] compared the residual stress under island, unidirectional, and alternating scanning strategies and concluded that chequerboard produced lowest residual stress. Lu et al. [28] studied the island size effect on residual stress in selective laser melting and found that island with a dimension of 5 mm × 5 mm exhibited lower residual stress than the islands with a dimension of 7 mm × 7 mm or 3 mm × 3 mm. Based on the island pattern, Ramos et al. [29] proposed the intermittent strategy to control the scanning order for the selective laser melting process, which could reduce heat accumulation by avoiding the flowing island adjacent to the two previous islands. Parry et al. numerally studied the effect of deposition part geometry on the residual stress distribution in selective laser melting. The results showed that when the scanning vector length was less than 3 mm, the laser scanning strategy played an important role in the residual stress, while when the scanning vector length was more than 3 mm, the laser scanning strategy had no significant effect on the residual stress. Parry et al. also concluded alternate scan vector directions produced lower residual stress, which was very useful for scanning strategy design [30,31].

Some studies have compared the residual stresses of direction-parallel, contour-parallel, and fractal patterns. Somashekara's [32] work showed that the raster pattern achieved the lower residual stresses than the spiral patterns, owing to the smaller thermal mismatch between the deposition material and the substrate as well as the lower secant-mismatch temperature rate at the top and bottom surface of the substrate. Ma et al. [33] numerally studied the maximum deformation under zig-zag and fractal scanning patterns in the selective laser melting process, and found the fractal scanning pattern exhibited smaller distortion. Yu et al. [34] experimentally studied the part distortion of raster, fractal, out-in spiral, and in-out spiral patterns in laser solid forming. The results suggested that the Hibert pattern possessed the lowest distortion followed by the in-out spiral pattern. Yan [7] compared the six representative patterns and concluded that the alternate-line pattern exhibited the minimum residual stress and warpage which was mainly dependent on the transient temperature gradients. Cheng et al. [21] evaluated the residual stress and deformation of the island, spiral, and zig-zag patterns with different angles of rotation in selective laser melting. Their findings showed that the out-in scanning pattern produced the maximum residual stress. Compared to other angles of rotation in zig-zag patterns, the 45° inclined line zig-zag pattern attained the lowest residual stresses and deformation. Despite those researches on the optimal pattern for reducing residual stress, most of them focus on the six typical patterns and the residual stress is still a challenge for AM. None of the existing patterns can perform well in all aspects: part strength, printing efficiency, applicability, surface accuracy, and reducing residual stress. Moreover, the relationships between transient temperature and residual stress are only qualitatively discussed to explain how the patterns affect residual stress [7,14,17]. Ren et al. applied two criteria to evaluate the localized and overall heat accumulation and proposed a way to find the optimal scanning pattern with minimum distortion [19]. However, the residual stress was not considered in this work. Hence new pattern

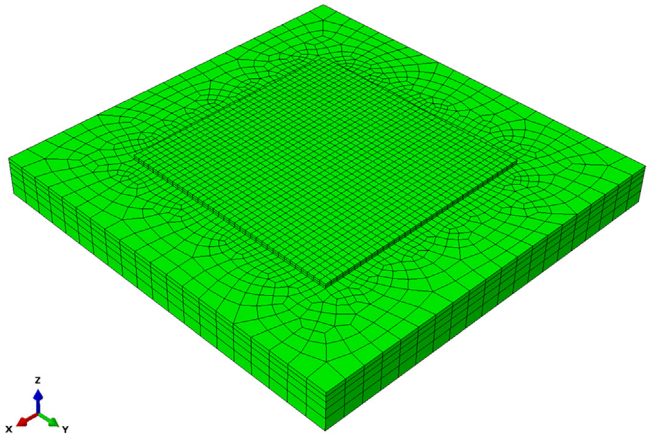

Fig. 2. Finite element model.

possessing multiple advantages, especially minimizing the residual stress, is required. Simple but quantitative correlations between temperature and residual stress are highly desired for comparing residual stresses under different patterns and optimizing AM pattern for industry context.

In this paper, a novel S-pattern is proposed for reducing residual stress in metal AM based on finite element (FE) analyses. The temperature, residual stress, and residual warpage under the new pattern are studied and compared with the results of five typical patterns. The correlations between the transient temperature and resulted residual stress are established for screening the patterns. In section 2, a 3D thermal-mechanical model is constructed to study the thermal field and residual stress distribution. The requirements of a pattern planning strategy for AM and the advantages and disadvantages of six typical patterns are analyzed. Accordingly, the S-pattern is proposed in section 3. Detailed results about the effect of patterns on the transient temperature field, residual stress, and warpage are presented in section 4. The correlation between temperature and residual stress is discussed in section 5. The main conclusions and future work are summarized in section 6.

2. Numerical methodology

Numerical modeling is a good way to study the complex thermo-mechanical performance with relations to process [35]. In this work, the FE method was used to scrutinize the effect of deposition patterns on the transient temperature field, residual stress, and warpage.

The model was one square deposition layer with the dimensions of 120 mm × 120 mm × 2.23 mm and a square substrate with the dimensions of 200 mm × 200 mm × 20 mm , as shown in Fig. 2. The deposition layer was divided into 36 × 36 × 2 elements and the average mesh size was 3.3 mm × 3.3 mm × 1.1175 mm. Relatively coarse mesh was assigned in the remaining part. Aluminum alloy 2319 was selected in this study. The melting range was 543−643 °C, and the mass density was assumed to be 2823 kg/m^3 and temperature independent. The temperature-dependent material properties of AA2319, such as the thermal conductivity coefficient, thermal expansion coefficient, temperature-dependent yield stress, are obtained from Ref. [36,37] and presented in Fig. 3.

The wire arc additive manufacturing process was simulated in ABAQUS 2018 and the paths of the adding material and heat input were defined by additive manufacturing plugin [39]. The elements are activated by the efficient method ṗrogressive element activationänd the process is controlled by the programmed time [39]. The uncoupled thermal-mechanical analysis included two stages: the thermal analysis and mechanical analysis. The procedure types were heat transfer (transient) and static general, respectively. There were many factors affecting the mignitude of residual stress, such as heat source, welding speed, pre-heat temperature [6]. To make the residual stress results under different patterns comparable, all the simulations were performed under the same parameters and the only variable was the deposition pattern.

Table 1
Parameters of the double-ellipsoid heat source.

a_f(mm)	a_r(mm)	b (mm)	c (mm)	Q (w)	f_f	f_r
4	6	5	5	5000	0.6	1.4

For the thermal analysis, the element type was eight-node linear brick (DC3D8). The conduction loss of the bottom surface is modeled by an equivalent convection coefficient (123 W/m^{2}k) [40–42]. While the other surfaces of the model were subjected to radiation and convection heat loss (radiation coefficient of 0.8 and convective coefficient of 8.5 W/(m^{2}K) [41,42]). A sufficiently long waiting time (5000 s) was used in the cooling stage to guarantee the model to be cooled down to room temperature naturally. The moving heat source was a double-ellipsoid heat source [43], where a_f and a_r were the length of the front and the rear ellipsoid of the heat source. b was the half width and c was the depth of the heat source. Q was the power input. The fraction factors of the heat flux in the front and rear parts were represented by f_f and f_r, respectively, and they held the relation that $f_f + f_r = 2$. The parameter values are shown in Table1.

After the thermal analysis, the transient temperature field output was imported into the mechanical analysis. The same FE mesh was used while the element type changed to C3D8R. The bottom of the substrate is mechanically fixed during the deposition process and then released after the model has been cooled down to room temperature to obtain the residual stress and deformation of the part. The phase transformation and the softening effect of the material are not considered in this model.

3. Deposition patterns in additive manufacturing

The most representative patterns used in AM are shown in Fig. 1(a–e). An ideal pattern should perform well in many aspects. The requirements of a pattern are summarized as follows [9].

1 Fewer pattern passes: the number of pattern passes depends on the number of starts and stops of energy source. More starts and stops will introduce larger cumulative deviations and lower deposition efficiency. Therefore, to improve the surface accuracy and deposition efficiency, the number of pattern passes should be minimized within each layer to reduce the number of starts and stops. With this regard a continuous pattern is preferable [9].
2 Fewer pattern elements: pattern elements are a sequence of line segments connecting to form the pattern, depending on the number of turns. The feedstock and heat input are easily excessive at the start and end positions of pattern elements. Excessive energy input will lead to voids [44]. Hence, the number of pattern elements should be minimized to improve the surface accuracy and final part quality.
3 Allowance to generate a weave pattern: the weave pattern can be generated by the cross passes among layers, which is beneficial for the component strength. The directional-parallel patterns allow generating weave patterns by changing the deposition orientation among different layers. The contour-parallel patterns are rarely used as fill patterns because each path is directly above each other on each layer. That can severely deteriorate the strength of the parts [7].
4 Minimum residual stress and warpage: the patterns have a great impact on residual stress and warpage which are the key challenges in terms of structural integrity and the final quality of

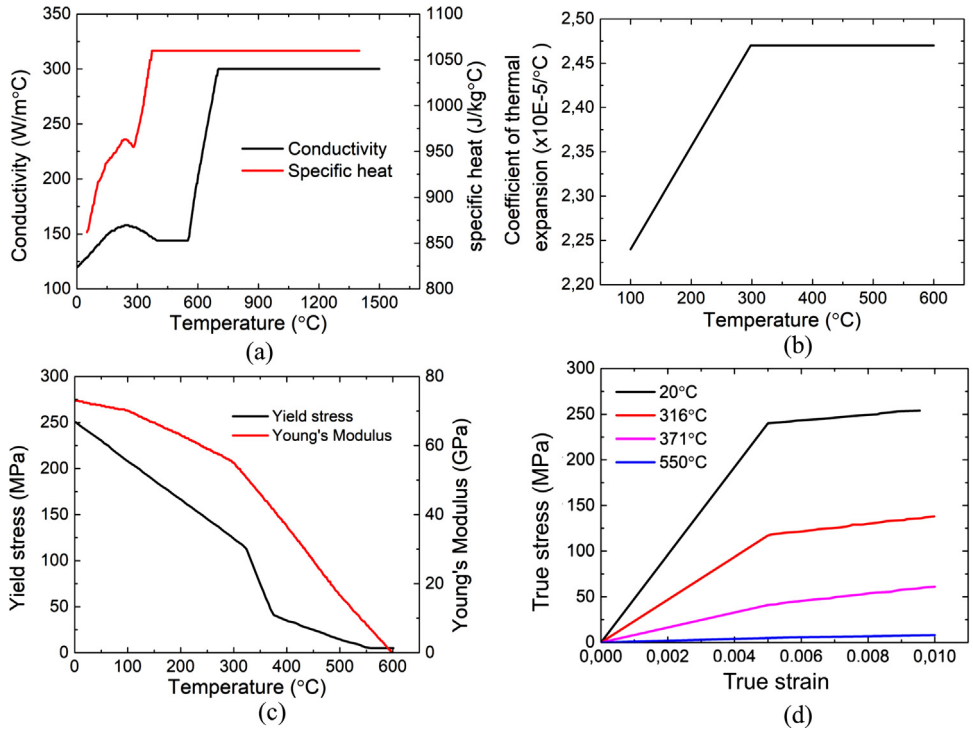

Fig. 3. Physical properties of AA2319: (a) thermal conductivity and specific heat, (b) coefficient of thermal expansion, (c) Young's modulus and yield strength, and (d) strain-hardening [36,38].

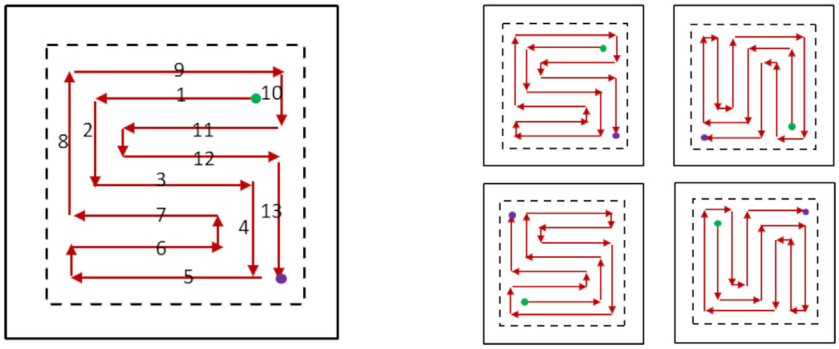

Fig. 4. The proposed deposition pattern: S pattern (a) One layer; (b) Multi-layer.

printed components in AM. The patterns which can achieve minimum residual stresses and warpage are favorable.

5 Adjustable pass length: the maximum residual stress can be reduced by shortening the length of the constituent passes of the pattern. Hence, adjustable pass length helps to reduce residual stress and warpage. Besides, adjustable pass length allows the pattern to be applied in different structures.

Table 2 summarizes the advantages and disadvantages of each pattern. As is shown, none of the existing patterns can possess all the advantages listed above. In this work, a new pattern, which combines multiple advantages of other existing patterns, is developed. Since the pattern is similar to the letter "S", it is named S-pattern, as shown in Fig. 4(a).

In Fig. 4(a), the start and end position of S pattern are marked in green and purple points. The numbers show the segment order. It is obvious that the S-pattern is continuous and has 13 line elements due to the turns, while the line elements numbers of the six typical patterns in Fig. 1(a)-(f) are 8, 8, 8, 16, 16, 51, respectively. Hence, the line element number of S-pattern is smaller than other contour-parallel patterns, which will lead to less deposition error.

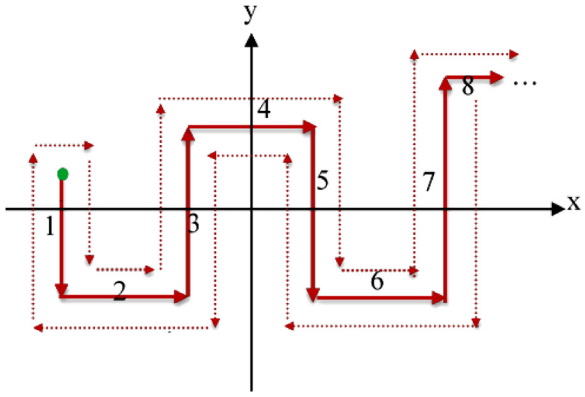

Fig. 5. S pattern in the shape made up of squares and rectangles.

The S-pattern allows generating a weave pattern among different layers, as shown in Fig. 4(b). For shapes making up of squares and rectangles, the matching S pattern can be generated by adjusting the length of passes and the number of turns, as shown in Fig. 5. Besides, it should be noted that the length of the horizontal passes,

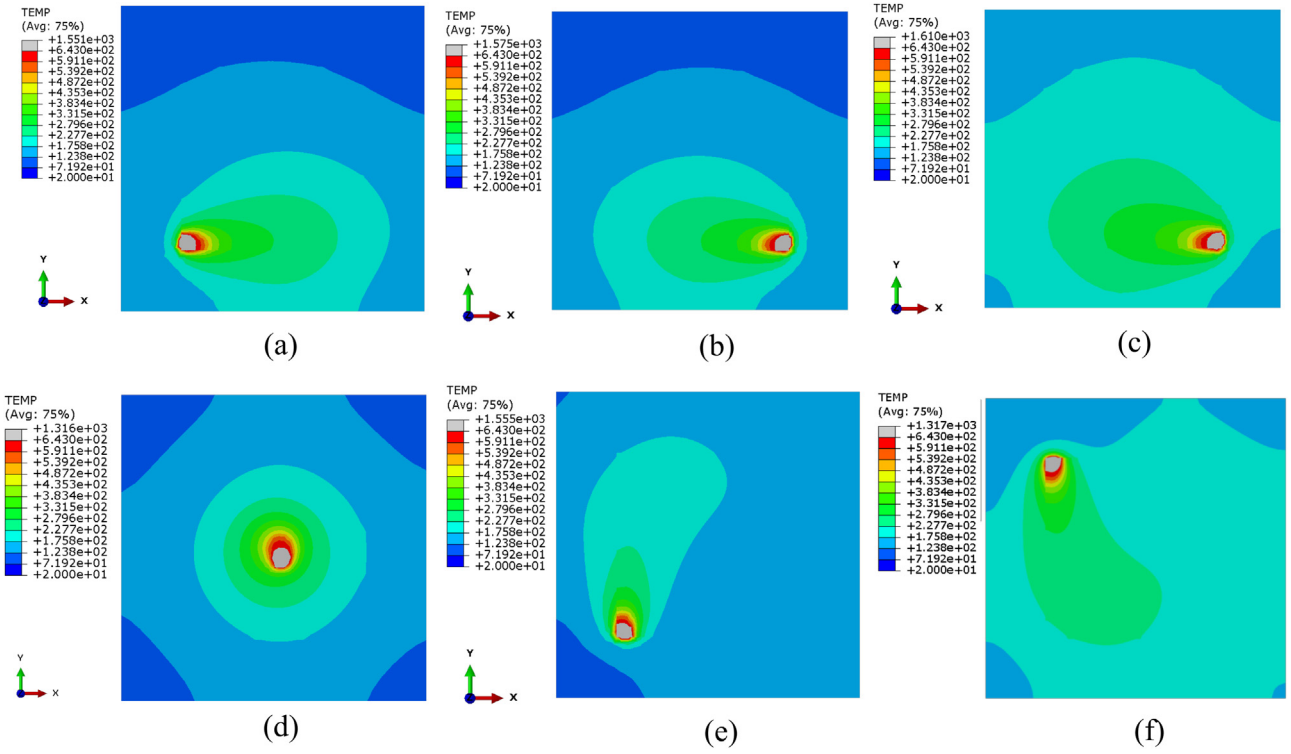

Fig. 6. The transient temperature distributions of all patterns at the end of deposition process (unit: °C, the color scale of all subfigures is from 20 °C to 643 °C (liquidus temperature)), (a) Zig-zag; (b) Raster; (c) Alternate-line; (d) Out-in spiral; (e) In-out spiral; (f) S.

like segments 2, 4, 6, should be consistent since the numbers of the vertical passes around the horizontal passes are the same. However, the S pattern is unsuitable for round, irregular, or other complex shapes. For large sizes or complex structures, it is recommended to divide into small squares or rectangles, then apply the S pattern to each sub-divided region. In this work, the effect of different patterns on the residual stress and warpage will be investigated. Since fractal patterns are presently used only in selective laser sintering [7], it is not considered.

4. Results

4.1. Transient temperature field

To study the temperature distribution history under different patterns, the transient temperature distributions of all patterns at the end of the deposition process are shown in Fig. 6. The grey color shows the melting zone. It is observed that the temperature gradients are relatively high near the melting pools and the deposition patterns have little effect on the melting pool size.

However, the deposition pattern remarkably influences the temperature distribution. For zig-zag, raster, and alternate-line deposition patterns (Fig. 6(a–c)), the temperature distribution characteristics are similar since all of these patterns are direction-parallel patterns. All of them are symmetrically distributed along the x-direction, and the high-temperature regions are near the bottom. The corresponding temperatures for raster and zig-zag patterns are very close, while the temperatures under alternate-line patterns are relatively high. Hence the alternate-line deposition pattern yields more uniform temperature distribution and lower temperature gradient. Similar to alternate-line pattern, the S-pattern (Fig. 6(f)) also achieves more uniform temperature distribution than others. It is because both alternate-line pattern and S-pattern have good heat transfer performance. The out-in spiral deposition pattern (Fig. 6(d)) produces a circular symmetry temperature distribution and concentrates a high-temperature area (over 400 °C) around the melting pool. Compared with other deposition patterns, it has a more concentrated heat distribution. The approximate diagonal symmetry temperature distribution is shown under the in-out spiral deposition pattern (Fig. 6(e)), which can effectively reduce the substrate distortion.

4.2. Residual stresses

In this work, the equivalent and maximum principal residual stress (σ_e and σ_1) are studied, since σ_e is relevant to plastic yielding and the σ_1 can be considered as a prime indicator of fatigue and fracture performance [45]. Figs. 7 and 8 show the top view σ_e and σ_1 distribution of the six deposition patterns after removing the constrains from the substrate base.

It is observed that, for all the patterns, the maximum σ_1 ($\sigma_{1,max}$) is at the edge of the square deposition area. This is because that the cooling rate at the edge of the square deposition area is higher than the interior and the temperature difference between the deposition area is larger. σ_1 is usually dependent on the longitudinal stress (parallel to the scan vector), which increases with scan vector length due to the presence of the thermal gradient parallel to the scan vector. Hence, $\sigma_{1,max}$ is at the square deposition area instead of the substrate. However, stress concentration happens around the four corners of the square deposition area, which is caused by the sudden change in the geometry of the mode. Hence, the maximum σ_e ($\sigma_{e,max}$) occurs near the four corners of the square deposition area at the substrate. The stress distributions of zig-zag (Fig. 7 and 8(a)) and raster (Fig. 7 and 8(b)) deposition patterns are pretty similar. Both of them have higher residual stress at the top. The out-in spiral (Fig. 7 and 8(d)) and in-out spiral (Fig. 7 and 8(e)) pattern produce circular symmetry stress distributions, and the residual stress of the out-in spiral is relatively higher. The alternate-line pattern (Fig. 7 and 8(c)) and S-pattern (Fig. 7 and 8(f)) show lower and more homogeneous residual stress

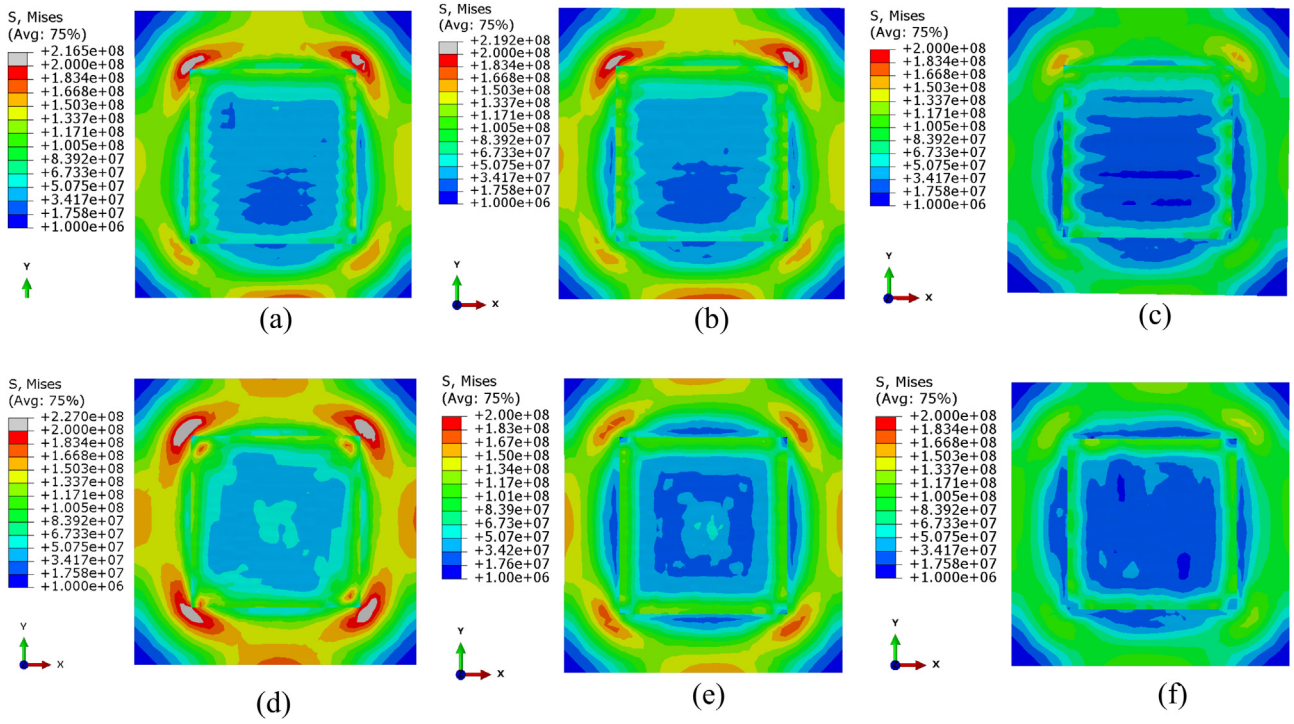

Fig. 7. Equivalent residual stress distribution of different deposition patterns, (top view, unit: Pa), (a) Zig-zag; (b) Raster; (c) Alternate-line; (d) Out-in spiral; (e) In-out spiral; (f) S.

Table 2
Summary of AM deposition patterns.

	Zig-zag	Raster	Alternate-line	In-out spiral	Out-in spiral	Hilbert	S
Continuous	√	×	×	√	√	√	√
Less pattern elements	○	√	√	○	○	×	○
weave pattern	√	√	√	×	×	√	√
Adjustable pass length	×	×	×	×	×	√	√
Lower residual stress	×	×	√	√	×	√	√
Lower warpage	×	×	○	√	○	○	○

Note: √-Positive; ×-Negative; ○-Medium (between the worst and best).

distributions than other patterns, in consistent with temperature distribution.

The normalized σ_e and σ_1 along the diagonal of the top surface of the deposition layer are plotted in Fig. 9. As indicated, for all patterns, the maximum magnitudes of residual stresses occur at both ends of the curves. For most of nodes, the S-pattern achieves the lowest normalized residual stresses, while the out-in spiral pattern induces the highest normalized residual stresses.

In order to compare the maximum residual stress, the $\sigma_{e,max}$ and $\sigma_{1,max}$ from largest to smallest are summarized in Fig. 10. For both σ_e and σ_1, the S-pattern has the minimum values. In detail, the $\sigma_{e,max}$ and $\sigma_{1,max}$ of S-pattern are 10.8 %–36.9 % and 9.5 %–32.7 % lower than those of the other five patterns, respectively.

4.3. Warpage

Warpage is another major challenge in the AM process, which can cause part distortion, loss of geometric tolerances, and cracks [46,47]. Moreover, residual stress and warpage often occur simultaneously because they interact with each other. Hence, in this work, the warpages under different patterns are also studied.

Fig. 11 shows the warpage in Z-direction under the six patterns. For all patterns, the warpage at the starting deposition position is larger due to the higher temperature gradient between the deposition material and the substrate at the initial position. The warpage distribution of the zig-zag pattern and raster pattern are similar and almost symmetric in the Y-direction. The warpage distribution of the out-in spiral and in-out spiral pattern are approximatively symmetric along the diagonal line of the substrate. For the out-in spiral pattern, the displacement of the center part is negative while the in-out spiral pattern leads to opposite results. Smaller warpage can be found under the alternate-line pattern, and positive and negative displacement are alternate corresponding to the pattern in the deposition area. For S pattern, the warpage of four corners and the first S contour is relatively high. Among all patterns, the in-out spiral pattern can achieve the most homogeneous warpage, since the heat is accumulated outward.

In order to compare the deformation of the substrate in Fig. 11, the U_z along the diagonal direction is normalized by the thickness of the substrate (d) and the normalized warpage U_z/d is summarized in Fig. 12. For the center part, all the curves collapse. At the edge, it is observed that the in-out spiral pattern achieves the minimum normalized warpage.

The normalized warpages at both ends are added to obtain the maximum normalized warpage $U_{z,max}/d$ of different patterns, which are plotted in Fig. 13. The in-out spiral pattern can achieve the lowest warpage, while the raster pattern produces the highest. There is no major difference between other patterns.

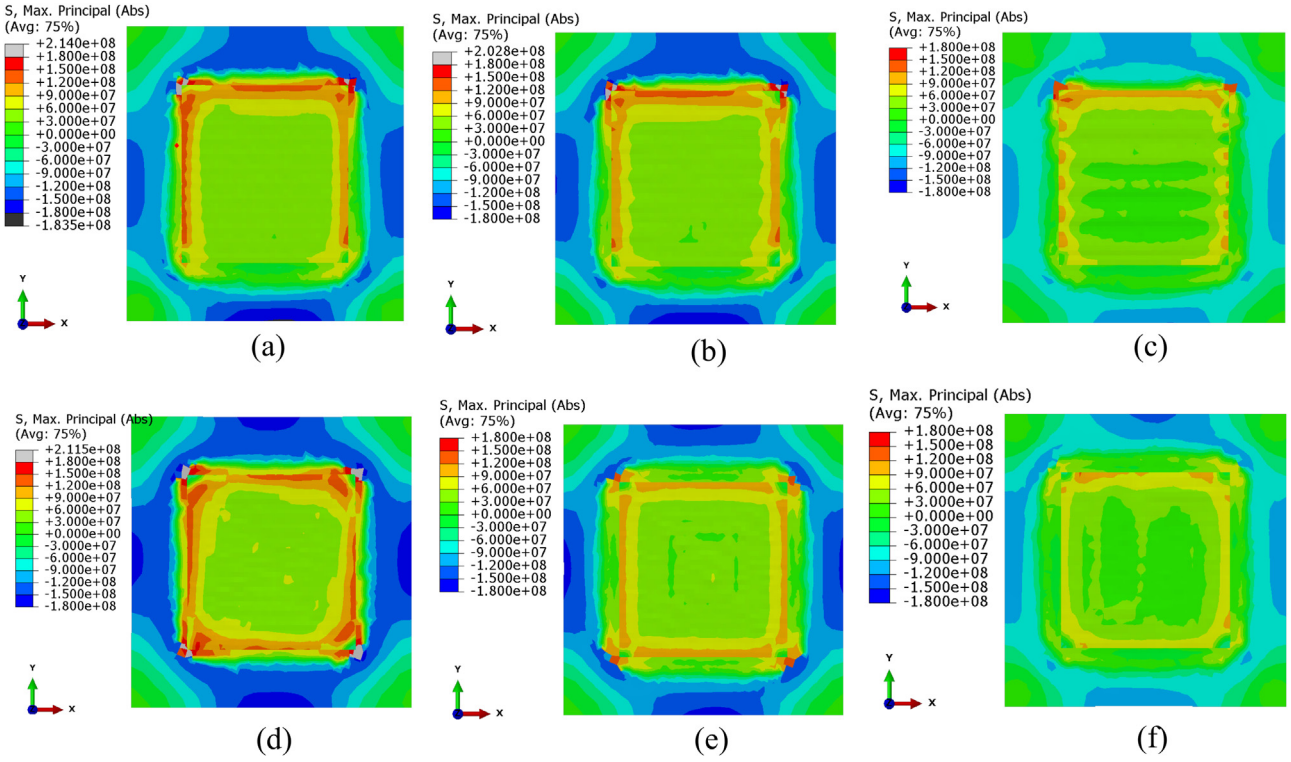

Fig. 8. Maximum principal residual stress distribution of different deposition patterns, (top view, unit: Pa), (a) Zig-zag; (b) Raster; (c) Alternate-line; (d) Out-in spiral; (e) In-out spiral; (f) S.

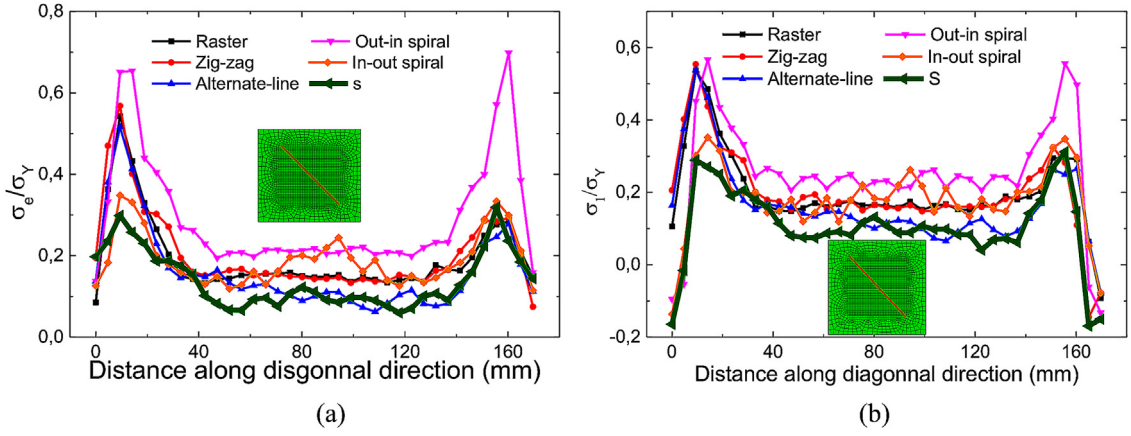

Fig. 9. Normalized residual stress along the diagonal direction of different patterns, (a) equivalent residual stress; (b) maximum principal residual stress.

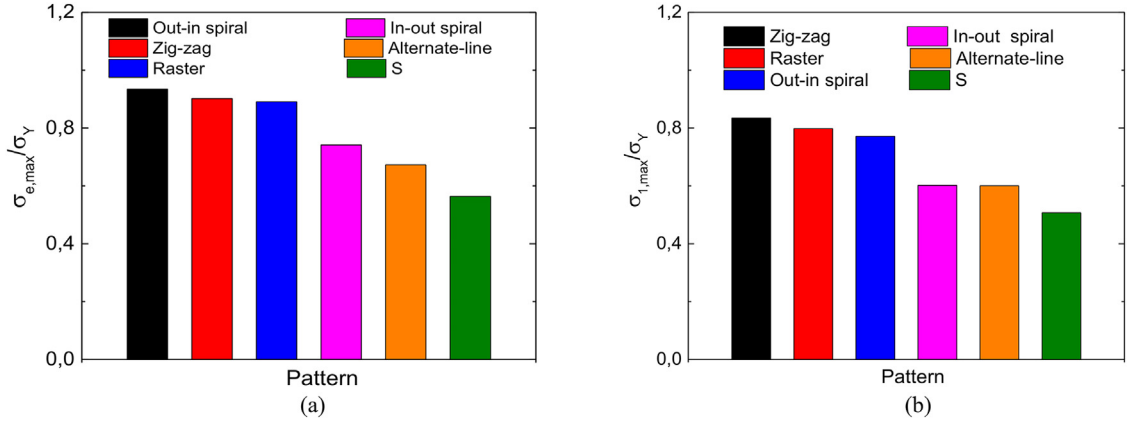

Fig. 10. Normalized maximum residual stress along the diagonal direction of different patterns, (a) equivalent residual stress (b) maximum principal residual stress.

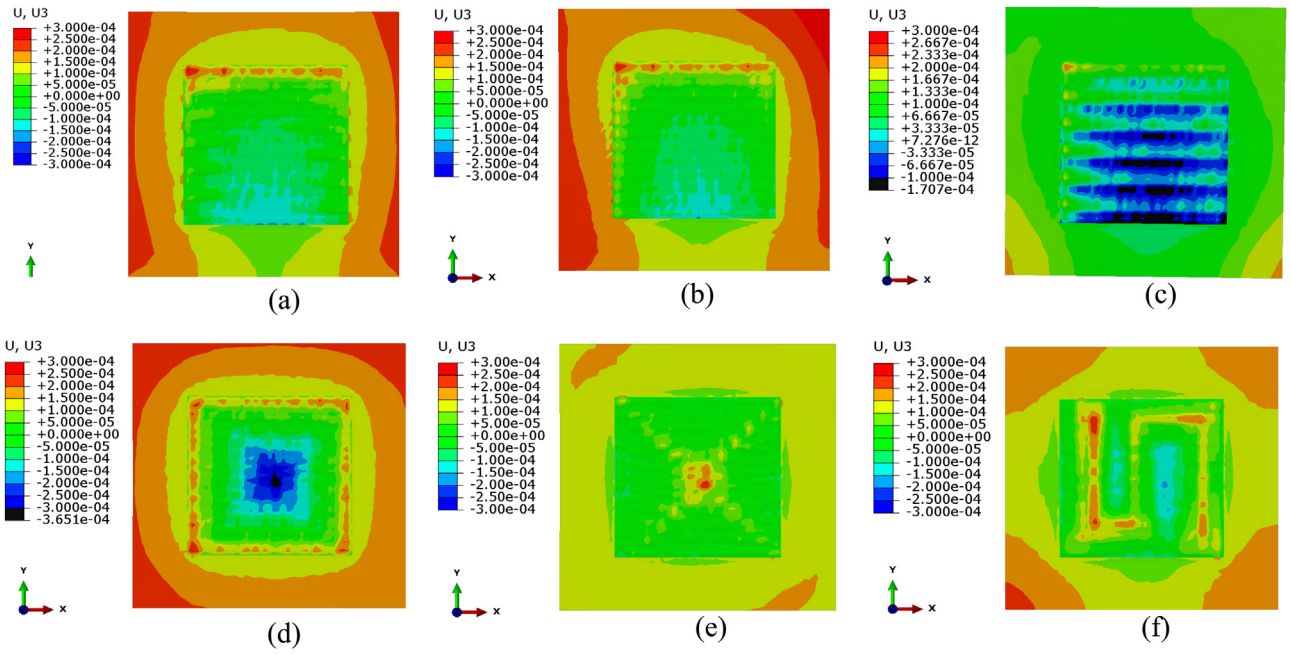

Fig. 11. Deformation distribution of different deposition patterns (unit: mm), (a) Zig-zag; (b) Raster; (c) Alternate-line; (d) Out-in spiral; (e) In-out spiral; (f) S.

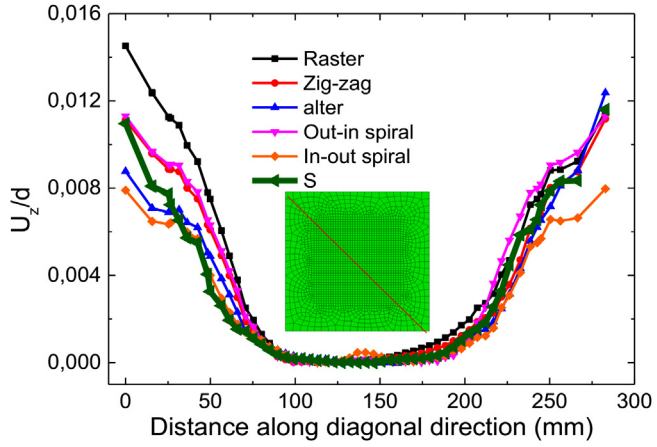

Fig. 12. Normalized warpage of different deposition patterns.

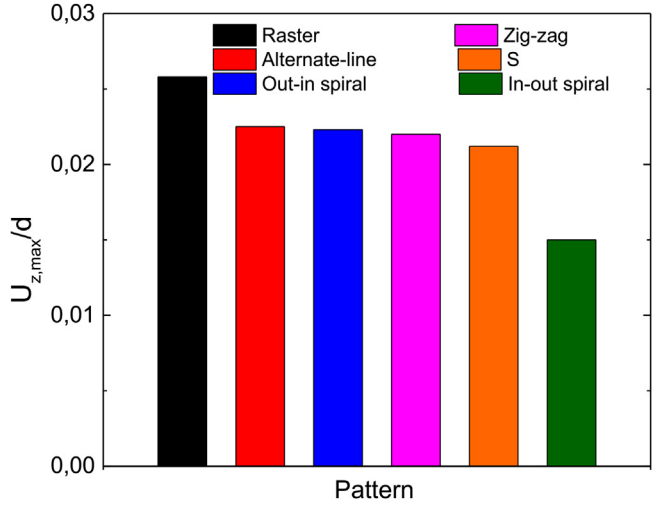

Fig. 13. Normalized maximum warpage among different deposition patterns.

5. Discussion

5.1. Residual stress for various patterns

As abovementioned, the deposition patterns show a significant influence on residual stress. To explore the origin of the residual stress differences in the six patterns, the temperature and final residual stress distribution results are analyzed from the perspective of deposition vector sequence, length and directions.

For S pattern, the prior deposition vectors (1,2,3,4,5) in Fig. 4 are more dispersed in the deposition area compared with other patterns, which helps to improve the efficiency of heat diffusion due to a greater surface area for heat dissipation. Hence the temperature distribution is more uniform instead of heat being concentrated in the deposition area. The prior deposition vectors (1,2,3,4,5) can also help to quickly preheat the whole substrate and reduce the magnitude of the temperature gradient for the next deposition vector. Furthermore, the S pattern is a continuous contour pattern, and the subsequent deposition vectors (6,7,8,9. . ...) are along the previous vectors. This will also prevent the heat from getting concentrated in the whole deposition process. In the same manner, the alternate-line pattern can achieve more homogeneous temperature distribution and lower residual stresses than other typical patterns. For the raster, zig-zag and out-in patterns, the subsequent deposition vectors are adjacent to the prior deposition vectors. Depending on the deposition vector sequence, the heat accumulated at one side or the center part of the deposition area over time, as shown in Fig. 6(a), (b) and (d). For the in-out pattern, the heat will accumulate around the edges due to the outward deposition vectors. However, the high heat dissipation efficiency at the edge will reduce heat accumulation. The temperature distribution under the in-out pattern becomes more uniform and thus the resultant residual stress is lower than that of the raster, zig-zag, and out-in patterns. In conclusion, the main reason that the S pattern can obtain the lower residual stress is that the deposition vectors are more uniformly distributed over time.

Parry et al. found that an increasing mean scan vector length could raise the overall magnitude of residual stresses. This is due to

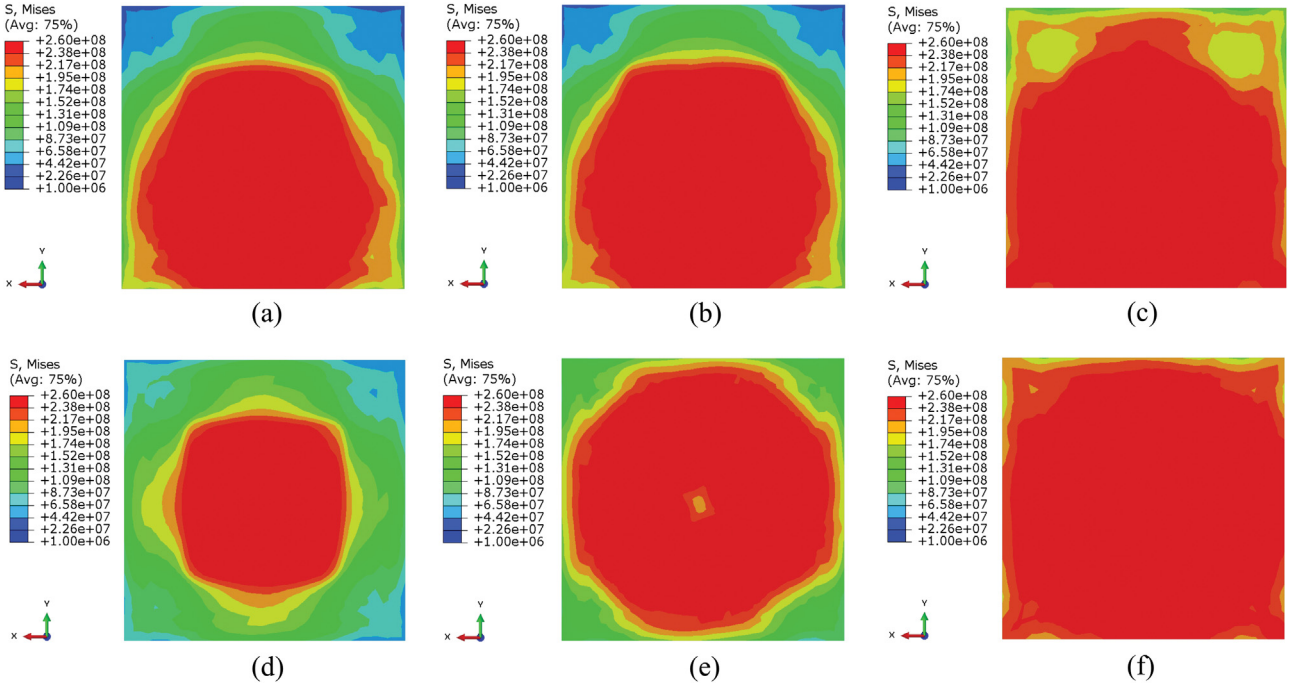

Fig. 14. σ_e distribution of the substrate before removing the constraint (bottom view, unit: Pa), (a) Zig-zag; (b) Raster; (c) Alternate-line; (d) Out-in spiral; (e) In-out spiral; (f) S.

Table 3
Mean and variance of deposition vector lengths for different patterns.

Patterns	Raster	Zig-zag	Alternate-line	Out-in spiral	In-out spiral	S
Mean (mm)	12	12	12	6.545	6.545	7.15
Variance	0	0	0	9.840	9.840	7.028

the rise of the longitudinal stress with scan vector length, which is the main contribution to stress because of its large thermal gradient parallel to the scan vector [30,31]. However, short scan vector length might cause a heat accumulation which may lead to high residual stress locally. Hence, lower fluctuations of scan vector length could reduce the risk of higher residual stress. The mean and variance of deposition vector lengths for different patterns in this work are summarized in Table 3. The mean deposition vector length of the S pattern is much shorter than that of raster, zig-zag and alternate-line patterns, which is one of the reasons why the residual stress of the S pattern is smaller. For out-in and in-out patterns, the mean deposition vector lengths are slightly smaller than that of S patterns. However, due to the very short deposition vectors in the center, their variances are larger than that of S pattern. This partly explains why the out-in and in-out patterns show higher residual stress than S pattern.

According to the above discussion, both the mean and variance of deposition vector lengths are important for residual stress. In Parry's work, it is recommended that to avoid the short adjacent deposition vectors (< 2.5 mm) and long deposition vectors (>5 mm) in selective laser melting. It is thus recommended to divide the large structures into small islands. This can be achieved by the S pattern, in which the deposition vector length is adjustable. The exact value of the critical deposition vector length remains to be studied for wire arc additive manufacturing. However, it should be noted that different residual stress distribution may still occur, like out-in spiral, in-out spiral or raster, alternate-line patterns, even though they possess the same mean or variance of the deposition vectors lengths. This may stem from the fact that the residual stresses are also dependent on the other factors.

Moreover, the alternate directions of scan vectors can also reduce the residual stress and produce a more anisotropic stress field in the component [31]. Compared to other patterns, the S pattern has a more uniform distribution of the deposition vector directions, and most of the adjacent vectors are in different directions, as shown in Fig. 5. Hence, it can be expected that the alternate directions of scan vectors help S pattern to achieve more anisotropic stress field and lower residual stress.

In summary, uniformly distributed deposition vector sequence, lower mean and variance of the deposition vector length, and alternate deposition vector directions favor reduced residual stress within a mesoscale region.

5.2. Correlations between the temperature and residual stresses

As mentioned before, the resulted residual stress and warpage are dependent on the temperature field. For mechanical analysis, there are two stages: before removing the constraint and after removing the constraint. To analyze the relationship between these two stages, the equivalent stress distributions of the substrate under six patterns before and after removing the constraint are shown in Figs. 14 and 15. It can be found that the corresponding stress fields before and after removing the constraint are correlated. The more uniform the stress distribution is in Fig. 14, the lower the residual stress is in Fig. 15. For example, the substrate residual stress distribution of the S-pattern is relatively homogeneous, while a heterogeneous distribution is observed in the out-in spiral pattern forming, see Fig. 14(d) and (f). After removing the constraint, the S-pattern shows the most homogeneous distribution of residual stress, while the out-in spiral pattern shows the

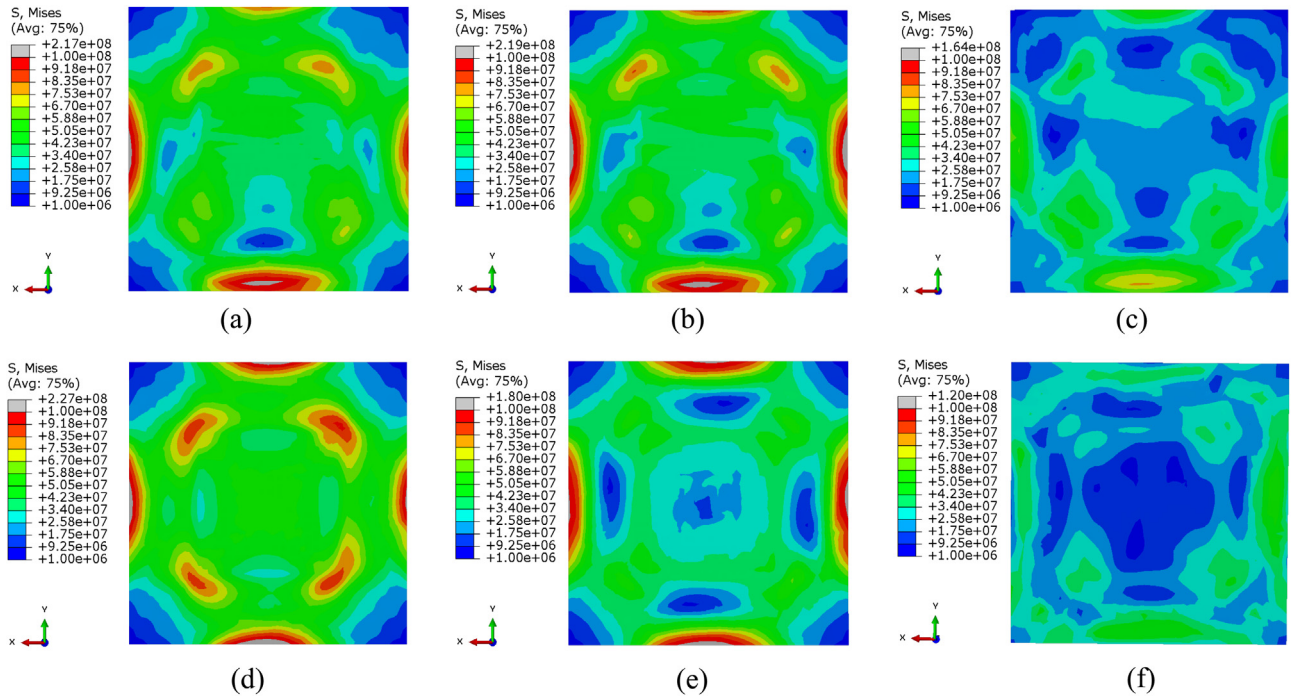

Fig. 15. σ_e distribution of the substrate after removing the constraints (bottom view, unit: Pa), (a) Zig-zag; (s) Raster; (c) Alternate-line; (d) Out-in spiral; (e) In-out spiral; (f) S.

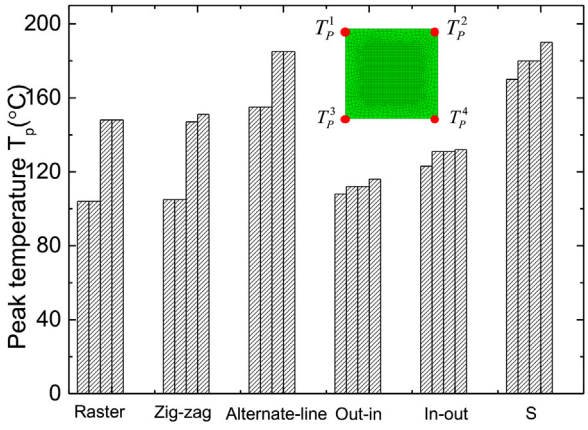

Fig. 16. Peak temperatures of the corners of different deposition patterns.

most non-uniform distribution of residual stress, see Fig. 15(d) and (f).

The above analysis suggests that the final residual stress is determined by the uniformity of the stress distribution before removing the constraint which depends on the magnitude of the edge stress since the residual stresses in the center portion are almost equal to the yield stress. Furthermore, the temperature distribution determines the uniformity of the stress distribution before removing the constraint and the edge stress distribution is related to the peak temperatures of edge nodes. Hence, the peak temperatures of the four corners, which represent the uniformity of the temperature distribution, can be used to analyze the residual stress distribution.

Fig. 16 summarizes the peak temperatures of the four corners under the six different deposition patterns. The peak temperatures of the raster is very close to that of the zig-zag, and same applies to the out-in and in-out spiral, owing to the similar deposition patterns. For raster, zig-zag and alternate-line patterns, the T_1^p and T_2^p are smaller than T_3^p and T_4^p, while all of the four peak temperatures are close for out-in spiral and in-out spiral patterns. It is because the contour-parallel patterns (in-out spiral, out-in spiral) can produce relatively uniform temperature distribution in all directions while the direction-parallel patterns (raster, zig-zag, and alternate-line) generate concentrated high temperature at one end. Since heat accumulation in the deposition area is depressed, the peak temperatures under alternate-line pattern and S-pattern are higher than those of other patterns.

To develop the relationships between the residual stress and the peak temperatures of the corners, the average peak temperatures and minimum peak temperatures under the different deposition patterns are plotted in Fig. 17(a and b). It can be seen that the order of $T_{p,ave}$ and $T_{p,min}$ are opposite to that of $\sigma_{e,max}$ and $\sigma_{1,max}$ (Fig. 10). Hence $\sigma_{e,max}$ and $\sigma_{1,max}$ are inversely correlated with the average peak temperature and the minimum peak temperature of corners, respectively. In other words, if the pattern produces higher peak temperature at the edge part, it will achieve lower residual stress. The correlations provide a simple yet effective approach to compare the residual stress under different patterns and guidance for optimizing pattern to reduce residual stress, which can be easily used in practice.

Based on the simulated thermal field, Ren et al. proposed an evaluation method to determine the optimal scanning pattern with minimal distortion [49]. In this method, two criteria were proposed: (1) the average and maximum temperatures within the moving melt-pool region at every unit simulation step; (2) temperature distribution variance of the whole part [49]. They were used to evaluate the extent of localized and overall heat accumulation. In our work, the maximum temperatures of the four corners of the substrate during the entire deposition process were used to evaluate the extent of overall heat accumulation. That is to say, the uniformity of temperature distribution of cuboid structure was represented by the peak temperatures of the four corners. The correlations between the peak temperature and the residual stress were developed. The localized heat accumulation was not considered in this work due to its dependence on the overall temperature distribution uniformity. It was also demonstrated in Ren's work that the largest value of temperature distribution variance of the whole

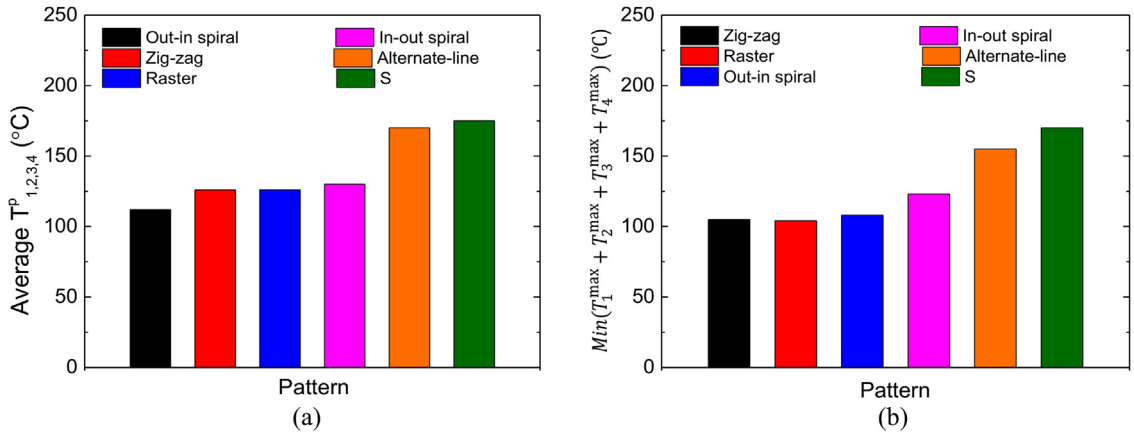

Fig. 17. (a) Average and (b) minimum peak temperatures of different deposition patterns.

part was positively correlated with the largest normalized melt-pool region mean temperature [49]. Compared with Ren's method, the evaluation method in our work is more straightforward and the maximum temperatures can be easily obtained in experiments, without simulations.

Since the heat transfer process and deposition process of directed energy deposition are similar to those of the powder bed additive manufacturing process, the S-pattern and correlations between the peak temperature and the residual stress can also be applied in the powder bed additive manufacturing process. However, the correlations are limited to the cuboid structure. For other geometries, although the residual stress distribution is also related to the uniformity of temperature distribution, the uniformity of temperature distribution should be re-evaluated, especially for complex structures. It should be noted that this work is a theoretical study, and potential collaborations on the experimental study are always welcome.

6. Conclusion

In this work, a so-called S-pattern was proposed. The residual stress and warpage of the S-pattern and the other five typical patterns were studied by the FE method. The results showed that the S-pattern achieved the minimum residual stress including equivalent residual stress and maximum principal residual stress due to more uniformly distributed deposition vector sequence, lower mean and variance of the deposition vector length, and alternate deposition vector directions, while the warpage of S-pattern was very close to the level of other patterns. In addition, the requirements of a pattern planning strategy for AM were summarized and the S-pattern could combine the various advantages of existing methods, such as continuous, fewer segments, adjustable pass length, and allowing generating a weave pattern among different layers. The S-pattern could be used not only in the directed energy deposition but also in the powder bed fusion additive manufacturing process. Hence, the S-pattern can be considered as the optimum one among the six deposition patterns and is promising for AM.

The residual stress distribution was determined by the uniformity of temperature field, which was correlated with the peak temperatures of corners. The equivalent residual stress and the maximum principal residual stress were inversely correlated with the average and the minimum peak temperature of corners, respectively. The correlations provided a simple yet effective approach for evaluating deposition patterns. Hence, the residual stress of different patterns could be compared by analyzing the peak temperature of the corners.

So far, only numerical studies were performed and conclusions were made based on the finite element analyses. In the near future, the experimental study of the S-pattern will be planned, and the effect of pass length of S-pattern on the residual stress should be considered to further optimize the pattern. The residual stress and warpage of the multi-layer model and cuboid structures with rectangular sections under the S-pattern will be studied.

Acknowledgments

This research is funded by the Chinese Scholarship Council and the Research Council of Norway through the Petromaks2 program (Project No. 281927) and the BIA Program (Project No. 269558)).

References

[1] E. Brandl, F. Palm, V. Michailov, B. Viehweger, C. Leyens, Mater. Des. 32 (2011) 4665–4675.
[2] J. Song, Y. Chew, L. Jiao, X. Yao, S.K. Moon, G. Bi, Addit. Manuf. 24 (2018) 543–551.
[3] B.E. Carroll, T.A. Palmer, A.M. Beese, Acta Mater. 87 (2015) 309–320.
[4] T. DebRoy, H.L. Wei, J.S. Zuback, T. Mukherjee, J.W. Elmer, J.O. Milewski, A.M. Beese, A. Wilson-Heid, A. De, W. Zhang, Prog. Mater. Sci. 92 (2018) 112–224.
[5] Y. Chew, J.H.L. Pang, G. Bi, B. Song, J. Mater. Process. Technol. 224 (2015) 89–101.
[6] J. Oliveira, T. Santos, R. Miranda,Prog. Mater. Sci. 107 (2020), 100590.
[7] W. Yan, Z. Yue, J. Feng, Rapid Prototyping J. 23 (6) (2017) 1057–1068.
[8] S. Routhu, D. Kanakanala, J. Ruan, X.F. Liu, F. Liou, in: International Design Engineering Technical Conferences (DETC 2010), Montreal, Quebec, Canada, January 1, 2010, pp. 415–423.
[9] D.H. Ding, Z.X. Pan, D. Cuiuri, H.J. Li, Int. J. Adv. Manuf. Technol. 73 (2014) 173–183.
[10] G.Q. Jin, W.D. Li, L. Gao, Robot. Comput.-Integr. Manuf. 29 (2013) 23–38.
[11] Y. Zhang, Y. Chen, P. Li, A.T. Male, J. Mater. Process. Technol. 135 (2003) 347–357.
[12] A.A. Ugla, O. Yilmaz, Arab. J. Sci. Eng. 42 (2017) 4701–4711.
[13] E. Foroozmehr, R. Kovacevic, Int. J. Adv. Manuf. Technol. 51 (2010) 659–669.
[14] N. Nazemi, R.J. Urbanic, Int. J. Adv. Manuf. Technol. 96 (2018) 4123–4143.
[15] D.H. Ding, Z.X. Pan, D. Cuiuri, H.J. Li, Robot Comput, -Integr. Manuf. 34 (2015) 8–19.
[16] C.Y. Wang Guilan, Zhang Haiou, Thin Solid Films 435 (2003) 124–130.
[17] K. Ren, Y. Chew, J.Y.H. Fuh, Y.F. Zhang, G.J. Bi, Mater. Des. 162 (2019) 80–93.
[18] Q. Wu, T. Mukherjee, C. Liu, J. Lu, T. DebRoy,Addit Manuf. 29 (2019), 100808.
[19] J.C. Snyder, K.A. Thole, in: ASME Turbo Expo: Turbomachinery Technical Conference and Exposition, Phoenix, June 17-21, 2019.
[20] F. Michel, H. Lockett, J. Ding, F. Martina, G. Marinelli, S. Williams, Robot. Comput.-Integr. Manuf. 60 (2019) 1–11.
[21] B. Cheng, S. Shrestha, K. Chou, Addit. Manuf. 12 (2016) 240–251.
[22] M.B.J.-P. Kruth, E. Yasa, J. Deckers, L. Thijs, J. Van Humbeeck, in: International Symposium on Electromachining (16th), Shanghai, China, April 19, 2010.
[23] J.P. Kruth, L. Froyen, J. Van Vaerenbergh, P. Mercelis, M. Rombouts, B. Lauwers, J. Mater. Process. Technol. 149 (2004) 616–622.
[24] J. Oliveira, A. LaLonde, J. Ma,Mater. Des. 193 (2020), 108762.
[25] D. Hagedorn-Hansen, M. Bezuidenhout, D. Dimitrov, G. Oosthuizen, S. Afr. J. Ind. Eng. 28 (2017) 200–212.

[26] A. Schröffer, J. Prsa, F. Irlinger, T.C. Lüth, in: IEEE International Conference on Robotics and Biomimetics, Kuala Lumpur, Malaysia, December 12-15, 2018, pp. 1894–1899.
[27] M.F. Zaeh, G. Branner, Prod. Eng. 4 (2010) 35–45.
[28] Y. Lu, S. Wu, Y. Gan, T. Huang, C. Yang, L. Junjie, J. Lin, Opt. Laser Technol. 75 (2015) 197–206.
[29] D. Ramos, F. Belblidia, J. Sienz, Addit. Manuf. 28 (2019) 554–564.
[30] L. Parry, I. Ashcroft, R. Wildman, Addit. Manuf. 25 (2019) 166–175.
[31] L. Parry, I. Ashcroft, R.D. Wildman, Addit. Manuf. 12 (2016) 1–15.
[32] M.A. Somashekara, M. Naveenkumar, A. Kumar, C. Viswanath, S. Simhambhatla, Int. J. Adv. Manuf. Technol. 90 (2016) 2009–2025.
[33] L. Ma, H. Bin, Int. J. Adv. Manuf. Technol. 34 (2006) 898–903.
[34] J. Yu, X. Lin, L. Ma, J. Wang, X. Fu, J. Chen, W. Huang, Mater. Sci. Eng. A 528 (2011) 1094–1104.
[35] A.J. Pinkerton,J. Laser Appl. 27 (2015), S15001.
[36] P. Michaleris, Z. Feng, G. Campbell, in: 1997 ASME Pressure Vessels and Piping Conference: Approximate Methods in the Design and Analysis of Pressure Vessels and Piping Components, Orlando, Florida, USA, January 1, 1997, pp. 91–102.
[37] M.G. Yuan, Y. Ueda, J. Eng. Mater. Technol. 118 (1996) 229–234.
[38] L. Sun, X. Ren, J. He, J.S. Olsen, S. Pallaspuro, Z. Zhang, Int. J. Adv. Manuf. Technol. 105 (2019) 2415–2429.
[39] Abaqus Analysis User's Guide, Abaqus 2018, Dassault Systèmes Simulia Corp., 2018.
[40] J. Ding, Thermo-mechanical Analysis of Wire and Arc Additive Manufacturing Process, Ph.D. Thesis, Cranfield University, UK, 2012.
[41] N. Nazemi, Identification of the Mechanical Properties in the Heat-affected Zone of Aluminum Welded Structures, Ph.D. Thesis, University of Windsor, Canada, 2015.
[42] M. Meco, S. Andreia, Joining of Steel to Aluminium Alloys for Advanced Structural Applications, Ph.D. Thesis, Cranfield University, UK, 2016.
[43] P. Ferro, F. Berto, N.M. James, Int. J. Fatigue 101 (2017) 421–429.
[44] J. Metelkova, Y. Kinds, K. Kempen, C. de Formanoir, A. Witvrouw, B. Van Hooreweder, Addit. Manuf. 23 (2018) 161–169.
[45] R. Martukanitz, P. Michaleris, T. Palmer, T. DebRoy, Z.K. Liu, R. Otis, T.W. Heo, L.Q. Chen, Addit. Manuf. 1-4 (2014) 52–63.
[46] K.J. Mercelis, Rapid Prototyping J. 12 (2006) 254–265.
[47] E.S. Gary, K. Lewis, Mater. Des. 21 (2000) 417–423.
[49] K. Ren, Y. Chew, Y.F. Zhang, G.J. Bi, J.Y.H. Fuh, J. Mater. Process. Technol. 271 (2019) 178–188.